Evidence of intrinsic impairment of osteoblast phenotype at the curve apex in girls with adolescent idiopathic scoliosis

Pearson, Mark; Philip, Ashleigh M; Nicholson, Thomas; Cooke, Megan; Grover, Liam; Newton Ede, Matthew; Jones, Simon

DOI:
10.1016/j.jspd.2018.11.016
10.1016/j.jspd.2018.11.016

Document Version
Peer reviewed version

Citation for published version (Harvard):
Pearson, M, Philip, AM, Nicholson, T, Cooke, M, Grover, L, Newton Ede, M & Jones, S 2019, 'Evidence of intrinsic impairment of osteoblast phenotype at the curve apex in girls with adolescent idiopathic scoliosis', *Spine Deformity*, vol. 7, no. 4, pp. 533-542. https://doi.org/10.1016/j.jspd.2018.11.016, https://doi.org/10.1016/j.jspd.2018.11.016

Evidence of intrinsic impairment of osteoblast phenotype at the curve apex in girls with adolescent idiopathic scoliosis

Mark J Pearson PhD [1†], Ashleigh M Philp PhD[1†], Hirah Haq[1], Megan E Cooke BSc[1], Thomas Nicholson BSc, Liam M Grover PhD[2], Matthew Newton Ede MBBS [3], Simon W Jones PhD[1*]

[1]Institute of Inflammation and Ageing, MRC-ARUK Centre for Musculoskeletal Ageing Research, School of Immunity, University of Birmingham, Birmingham, UK.

[2]School of Chemical Engineering, University of Birmingham, Birmingham, B15 2TT UK.

[3]Royal Orthopaedic Hospital NHS Trust, Bristol Road South, Birmingham, UK..

[†] These authors contributed equally to this work

*Corresponding author:

Dr Simon W. Jones

Institute of Inflammation and Ageing

MRC-ARUK Centre for Musculoskeletal Ageing Research

School of Immunity

University of Birmingham

Birmingham, UK.

E-mail:s.w.jones@bham.ac.uk

Tel: +44 121 3713224

Funding: Birmingham Orthopaedic Charity

Ethical approval: The study was approved by the Royal Orthopaedic Hospital Ethical Review panel (ROH16/002).

		MJP	AMP	HH	MEC	TN	LMG	MNE	SWJ
Substantial contribution to	**the conception or design of the work**							X	X
	the acquisition analysis, interpretation of data for the work	X	X	X	X	X	X		
Drafting the work or revising it for important intellectual content		X	X	X	X	X	X	X	X
Final approval		X	X	X	X	X	X	X	X

Key points

1. Osteoblasts at the convex side of the curve apex in AIS patients exhibit greater metabolic capacity

2. Convex osteoblasts from the curve apex exhibit greater mineralisation capacity than concave osteoblasts

3. Osteoblasts at the curve apex exhibit differential expression of wnt signalling genes in AIS patients

Abstract (300 words)

Study design

An observational descriptional study based on a single cohort of patients.

Objective

To determine whether spinal facet osteoblasts at the curve apex display a different phenotype to osteoblasts from outside the curve in adolescent idiopathic scoliosis (AIS) patients.

Summary of background data

Intrinsic differences in the phenotype of spinal facet bone tissue and in spinal osteoblasts have been implicated in the pathology of AIS. However, no study has compared the phenotype of facet osteoblasts at the curve apex compared to outside the curve in AIS patients.

Methods

Facet spinal tissue was collected peri-operatively from 3 sites, the concave and convex side at the curve apex and from outside the curve (non-curve) from n=3 AIS female patients aged 13-16. Spinal tissue was analysed by MicroCT to determine Bone Mineral Density (BMD) and trabecular structure. Primary osteoblasts were cultured from concave, convex and non-curve facet bone chips. The phenotype of osteoblasts was determined by assessment of cellular proliferation (MTS assay), cellular metabolism (alkaline phosphatase and Seahorse Analyser), bone nodule mineralisation (Alizarin red assay) and the mRNA expression of Wnt signalling genes (qRTPCR).

Results

Convex facet tissue exhibited greater BMD and trabecular thickness, compared to concave facet tissue. Osteoblasts at the convex side of the curve apex exhibited a

significantly higher proliferative and metabolic phenotype and a greater capacity to form mineralised bone nodules, compared to concave osteoblasts. mRNA expression of SKP2 was significantly greater in both concave and convex osteoblasts, compared to non-curve osteoblasts. The expression of SFRP1 was significantly down-regulated in convex osteoblasts, compared to either concave or non-curve.

Conclusions

Intrinsic differences that affect osteoblast function are exhibited by spinal facet osteoblasts at the curve apex in AIS patients.

Level of evidence

Level IV

Introduction

Adolescent idiopathic scoliosis (AIS) is the most common paediatric spinal deformity. Characterised as lateral curvature of the spine in children aged between 10-18 years old it affects between 2-3% of this population [1]. It is a highly heterogeneous condition with some patients exhibiting rapidly progressive aggressive curves. Critically, AIS patient management procedures including bracing, growth modulation and fusion are all associated with significant morbidity [1-3]. Therefore, identifying the central pathogenic drivers will facilitate the development of pharmacological therapeutics and may also help to identify predictive markers of aggressive curves to inform clinicians and patients.

Importantly, there is now increasing evidence to support a role for abnormal spinal bone tissue as a primary intrinsic driver of AIS pathogenesis and a key determinant of curve progression [4-6]. It is well known that AIS patients exhibit lower lumbar spine bone mineral density (LSBMD) [7-9] and altered vertebral growth [10-12], resulting in disparity between the growth of anterior and posterior vertebrae with rotational lordosis. Furthermore, several studies have now provided evidence for the dysregulation of key molecular signalling pathways that are known regulators of bone mass. Genetic studies in girls with AIS have shown associations between LSBMD with polymorphisms of osteoprotegrin (OPG), the decoy receptor for RANKL, which is secreted by osteoblasts and reduces osteoclast activity [13]. Increased serum concentrations of RANKL and an increase in the RANKL:OPG ratio have been reported in patients with AIS and were found to be negatively correlated to LSBMD [9]. In addition, it was recently demonstrated *in vitro* that, in contrast to healthy osteoblasts, osteoblasts isolated from AIS patients were insensitive to the pro-proliferative effect of melatonin stimulation [14], suggesting an intrinsic dysfunction

in melatonin signalling may exist in human AIS spinal bone tissue. Notably, in animal models of idiopathic scoliosis, development of idiopathic scoliosis-like changes is associated with reduced systemic levels of melatonin, whilst melatonin administration prevents scoliosis development in both chick and rodent models [15-18]. Despite these studies, no study has compared the phenotype and function of AIS facet osteoblasts at the curve apex compared to facet osteoblasts outside of the curve. Intrinsic differences in osteoblast phenotype at the apex of the curve may be central to mediating localised abnormal vertebral growth which drives curvature. Therefore, the aim of this study was to examine the phenotype of spinal bone tissue and isolated osteoblasts from the convex and concave side of the curve at the curve apex and from outside the curve in patients with AIS.

Methods

Ethical Approval and Subject Recruitment

AIS female patients aged 13-16 yrs old (n=3) scheduled for corrective spinal surgery were recruited following ethical apporoval (ROH16/002). Consent was obtained from all patients and their families. Peri-operatively, facet spinal tissue was collected from 3 sites, the convex and concave side at the curve apex and from outside the curve (non-curve). Pre-operative x-ray radiographs of the spine were analysed to determine Cobb angle.

MicroCT analysis

Bone gross structural parameters were determined using a Bruker Sky scan 1172 (e2v technologies plc, Chelmsford, UK). Scans were performed at 59 kV and 100 uA with a 0.5 mm aluminium filter. Pixel size was set to 13.52 µm, with a rotation step of 0.3° and exposure time of 1750 ms. Reconstruction was performed using NRecon software version 1.7.1 (SkyScan, e2v technologies plc, Chelmsford, UK). Analysis was performed using CTAn software version 1.15.4 (Bruker, Chelmsford, UK). A region of interest was defined to exclude cortical bone from the analysis. For bone mineral density, hydroxyapatite phantoms of 250 and 750 mg.cm-1 (Bruker) were scanned and reconstructed in the exact same conditions as the bone samples. The attenuation of each phantom was calculated and used to calibrate the software to determine BMD

Isolation and culture of primary spinal osteoblasts

Facet bone chips were washed three times in Dulbecco's Modified Eagles Media (DMEM, Sigma Aldrich, UK) containing 100U/mL penicillin, streptomycin and

cultured in differentiation media (DMEM, 10% FBS, 100Units/mL Penicillin Streptomycin, 2mM L-Glutamine, 1% NEAA, 2mM b -glycerophosphate, 50ug/mL L-Ascorbic Acid, 10nM Dexamethasone). Media was changed every 3 days and bone chips removed upon the appearance of osteoblasts.

Osteoblast cellular proliferation

Primary osteoblasts from non-curve, convex and concave bone chips were cultured at 4000 cells/well in 96-well plates over a timecourse up to 21 d. Proliferation was determined using the CellTiter 96 Aqueous One Solution Cell Proliferation Assay kit (Promega, USA) as per the manufacturer's instructions.

Seahorse XFe96 analysis of osteoblast metabolic function

A Seahorse XFe96 analyser (Agilent Technologies, Santa Clara, California, United States) was used to conduct a Seahorse XF Mito Stress Test in accordance with the manufacturer's recommendations. Osteoblasts (2.5×10^4 cells per well) were seeded to 0.2 % gelatin-coated Seahorse XFe96 Cell Culture Microplates. Treatment conditions were assayed in triplicate.

Alkaline Phosphatase (ALP) Assay

Osteoblasts were lysed in 150mM Sodium Chloride, 1% triton x-100, 50mM Tris, pH 8.0 containing protease and phosphatase inhibitor cocktails (Sigma Aldrich, Poole, U). Lysate protein concentration was determined by Bradford assay [19]. To 10µl osteoblast lysate, 100µl of alkaline phosphatase substrate containing *p*-nitrophenylphosphate (pNNP) was added and incubated for 15 min at 37°C before

being stopped by the addition of 20µl 0.1M sodium hydroxide. Human alkaline phosphatase was used as a standard and absorbance was measured at 405nm.

Alizarin Red Mineralisation Assay

Osteoblast mineralisation was determined by Alizarin Red staining, as previously described [20-22]. In brief, upon reaching confluence osteoblasts were grown for a further 3 weeks and then stained with 0.5% alizarin red solution (0.5% Alizarin Red, 1% ammonia solution, pH 4.0) for 10 min. Cells were washed in PBS and destained using 10% cetyl pryridium chloride (Sigma, UK) for 10 min. The absorbance of the supernatant was measured at 550 nm on a platereader.

Gene expression analysis

Total RNA was isolated from convex, concave and non-curve primary facet joint osteoblasts using Trizol reagent (Qiagen, UK). The mRNA expression of 84 Wnt-signalling genes was determined by qRT-PCR using an RT2 Profiler PCR array (Qiagen, UK) as per the manufacturer's instructions. The mRNA expression of **SKP2 and SFRP1** was determined by qRT-PCR using Taqman probes (Dharmacon, GE LifeSciences, UK) and normalised to 18S.

Pathway Analysis

Pathway analysis was conducted on mRNAs from the RT2 Profiler PCR array that were differentially expressed >2-fold either between convex and concave, or between non-curve and convex/concave osteoblasts. Pathway analysis was performed using Ingenuity Pathway Analysis software (www.ingenuity.com). In brief, a core functional analysis was performed on the differentially expressed genes to

visualise the alignment of the differentially expressed genes to the canonical Wnt signalling pathway and to generate novel gene network maps.

Statistical analysis

Data was analysed by ANOVA performed using IBM SPSS Statistics v22 and GraphPad Prism, with Bonferroni's multiple comparison test used where appropriate. Significance was accepted as $p < 0.05$.

Results

1. Characterisation of patients and patient samples

Pre-operative radiographs revealed Cobb angles between 105 and 50º (**Figure 1A**). MicroCT analysis of the peri-operative bone tissue samples (**Figure 1B**) was performed in order to determine bone mineral density (BMD) and structural parameters of trabecular thickness (Tb.Th) and trabecular number (Tb.N). BMD and Tb.Th were found to be greater in the convex bone tissue, compared to the patient-matched concave bone tissue in each of the three patients analysed (**Table 1**).

2. Osteoblasts from the convex side of the curve apex in AIS patients exhibit a greater metabolic proliferative phenotype.

Next, we isolated osteoblasts from the bone chips taken from the concave and convex side of the curve apex and from outside of the curve, and examined their metabolic proliferative phenotype. Non-curve, concave and convex osteoblasts (n=3 patients) were cultured in growth media alone or growth media supplemented with melatonin (120 pg/ml). MTS reagent used to determine cell proliferation. As expected, over the course of 21 days there was a significant increase in osteoblast cell proliferation. However, convex osteoblasts proliferated at a greater rate, showing significantly ($p<0.001$) greater proliferative activity at 21 days, compared to either concave or non-curve osteoblasts (**Figure 2A**).

Compared to media alone, there was a small but significant effect of melatonin in promoting the proliferation of convex ($p<0.05$), concave ($p<0.001$) and non curve ($p<0.01$) osteoblasts. However, there was no significant difference between the different osteoblast cell types in their responsiveness to melatonin (**Figure 2B**).

We next interrogated the metabolic functional phenotype of the osteoblasts by determining oxidative and glycolytic metabolism using a Seahorse XF Analyser mitochondrial stress test. Analysis of metabolic function revealed that convex osteoblasts displayed significantly greater basal and maximal oxygen consumption rate (OCR), compared to either concave or non-curve osteoblasts (**Figure 3A and 3B**). In addition to elevated oxidative phosphorylation, convex osteoblasts also exhibited increased extracellular acidification rate, indicative of elevated glycolytic metabolism (**Figure 3C**).

3. Convex osteoblasts from the curve apex exhibit greater mineralisation capacity than concave osteoblasts

We next examined whether the greater metabolic activity of convex osteoblasts was reflected in a greater functional ability to mineralise bone. Since the enzyme alkaline phosphatase (ALP) provides inorganic phosphate to promote mineralisation we first assessed ALP activity in convex, concave and non-curve osteoblasts over a period of 7 days of culture. Over the duration of the 7 days, convex osteoblasts exhibited significantly greater alkaline phosphatase activity, compared to either concave or non-curve osteoblasts (**Figure 4A**). To determine bone mineralisation, we cultured convex and concave osteoblasts in 24-well plates for a further 14 days upon reaching confluence and stained for mineralised bone nodules using Alizarin Red. Both osteoblast cell types were capable of forming mineralised bone nodules. However, significantly greater mineralisation was exhibited by the convex osteoblasts, compared to the concave osteoblasts (**Figure 4B**).

4 Convex osteoblasts from the curve apex exhibit differential expression of Wnt signalling genes

To determine whether osteoblasts from the convex and concave side of the curve apex exhibited a different transcriptomic phenotype compared to non-curve osteoblasts we initially performed a broad expression profile of 84 Wnt signalling pathway components and mediators (including Wnt ligands, receptors and Wnt target genes) using a RT2-profiler array (Qiagen, UK). In total, 62/84 genes were detected, of which 17 were differentially expressed >2-fold between convex and concave osteoblasts (Table 2).

Based on fold-change and absolute expression we then selected the genes SKP2 (S-phase kinase-associated protein 2) and SFRP1 and validated their expression in non-curve, convex and concave osteoblasts from n=3 patients. SKP2 was found to be significantly increased by approximately 2-fold in both concave and convex osteoblasts, compared to non-curve osteoblasts. Expression of SFRP1 was comparable between concave and non-curve osteoblast, but was significantly down-regulated in convex osteoblasts (**Figure 5A**).

We then utilised pathway analysis software to visualise the alignment of the differentialy expressed mRNAs to the canonical wnt signalling pathway. With the focus on SKP2 and SFRP1, network analyses generated novel network maps, which showed the central role of both SKP2 and SFRP1 as regulators of multiple components of the wnt signalling pathway (**Figure 5B**).

Discussion

This study is the first to examine the intrinsic differences in the functional phenotype of spinal osteoblasts at the curve apex compared to non-curve in patients with AIS. Furthermore, this is the first study to identify two candidate genes, namely SKP2 and SFRP1, that are differentially expressed in osteoblasts at the curve apex.

On the basis that differences in the proliferative activity of osteoblasts at the curve apex might drive bone curvature we first examined the *in vitro* proliferation of osteoblasts over a timecourse of 21 days. Notably, convex osteoblasts displayed greater proliferative capacity compared to either concave or non-curve osteoblasts. However, we observed no difference in the responsiveness of the different osteoblast cell types to the presence of melatonin in the culture media. Although systemic levels of melatonin are not reported to be different in AIS patients [23,24], it has been shown that melatonin induces the proliferation of normal healthy osteoblasts but not AIS osteoblasts [14]. Our finding that there was no difference between osteoblasts from outside the curve and those at the curve apex in responsiveness to melatonin suggests that it is unlikely that intrinsic differences in melatonin signalling play a central role in AIS curvature.

In addition to the greater proliferative capacity, convex osteoblasts also exhibited greater metabolic activity than either concave or non-curve osteoblasts, with higher basal and maximal respiratory capacity. This greater metabolic acitivty was also reflected in greater alkaline phosphatase activity of convex osteoblasts in culture, which led to greater mineralised bone nodule formation. Notably, MicroCT analysis showed that BMD was comparively higher in bone facet tissue from the convex side of the curve, than in either concave or non-curve bone facet tissue. Although several studies have reported lower lumbar spine BMD in patients AIS patients [9,12,25,26] it is

unclear if the differential in mineral deposition *per se* between convex and concave bone tissue and between convex and concave osteobalasts at the curve apex plays a mechanistic role in mediating AIS spinal curvature. Perhaps more likely, the differential mineralisation is a marker of more active osteoblasts on the convex side of the curve driving greater bone formation

In attempting to understand the molecular basis for these functional differences our study has idenfiied two Wnt signalling genes, SKP2 and SFRP1, that are differentially expressed in osteoblasts at the curve apex. SFRP, a 35 kDa prototypical member of the SFRP family, was found to be signifjcanflty downregulated in convex osteoblasts, compared to either concave or non-curve osteoblasts. Critically, SFRP1 acts as a biphasic modulator of Wnt signalling [27,28], counteracting Wnt-induced effects at high concentrations and promoting them at lower concentrations. As such, SFRP1 is considered a crtical regulator of cellular proliferation and migration and its differential expression has been implicated in the the development of multiple cancers, including pancreatic [29], gliobastoma [30] and colorectal [31,32], and in musculoskeletal connective tissue disorders [33,34]. Therefore, the reduced expression of this critical modualtor of Wnt signalling activity may have important implications for the homeostatic control of osteoblast activity and ultimately bone formation at the curve apex.

SKP2 was found to be more highly expressed in both convex and concave osteoblasts, compared to non-curve osteoblasts. SKP2 has been shown to target RUNX2 [35], an essential osteoblast transcription factor [36-41], for ubiquitin mediated degradation, thus regulating osteogenesis [35]. Therefore, the significant increase in expression of SKP2 in osteoblasts at either side of the curve apex could indicate a pathological impact on osteogenesis. These findings add significant weight to the

role of dysfunctional wnt signalling pathway in AIS pathogenesis. Previously, it has been reported that loss of function mutations in the Wnt mediator gene PTK7 in zebrafish leads to malformed vertebrae [42] and missense PTK7 variants have been idenfified in AIS patients [42]. Furthermore, varants in VANGL1, a regulator of WNT/planar cell polarity (PCP) signalling, were recently identified in a cohort of 157 moderate to severe AIS patients [43].

This study has a number of limitations. Given the study design it is not possible to determine whether the changes we have observed here are causative. It is conceivable that these differences in osteoblast phenotype at the curve apex are secondary to changes in paraspinal muscles that control spinal stability. However, to determine whether such differences are causative is inherently difficult. Collecting spinal tissue samples from patients at the onset of disease, prior to spinal curvature, is currently not feasible because there are no biomarkers to diagnose patients with very early stage disease.

It should also be noted that this study is observational and is based on a small cohort of patients. It is important therefore that these findings are validated in a larger patient cohort. Furthermore, given the small patient size it was not possible to determine a relationship between osteoblast phenotype and curve severity, which could help to ascertain whether the effects reported here causative. Finally, it is was only possible to obtain relatively small bone tissue samples, which limited the ability to perform extensive omic profiling and functional analyses of osteoblasts.

Despite these limitations, this study provides evidence for the first time that intrinsic differences that affect osteoblast function are exhibited by spinal facet osteoblasts at the curve apex in AIS patients. Such differences may play a causative role in the development of AIS, and therefore warrant further study in a larger patient cohort.

Figure legends

Figure 1. AIS patient radiographs and MicroCT scans of collected face spinal tissues. (**A**) Pre-operative radiographs of AIS patients used to determine cobb angle. Peri-operatively, facet spinal tissue was collected from 3 sites for each patient, namely the convex (black arrowhead) and concave (white arrowhead) side at the curve apex and from outside the curve (grey arrowhead; non-curve). (B) MicroCT reconstructed facet bone tissue samples. Samples were scanned at 59 kV and 100 uA with a 0.5 mm aluminium filter and pixel size at 13.52 µm **(**Bruker Skyscan 1172). Reconstruction was performed using the NRecon software v1.7.1 (SkyScan). The white scale bar represents 3 mm length.

Figure 2. Comparison between the proliferation of osteoblasts from either side of the curve apex with non-curve osteoblasts. (**A**) Timecourse of 21 days of the proliferation of convex, concave and non-curve primary osteoblasts from n=3 patients. Osetoblasts were seeded at 4000 cells/well in 96-well plates. At each timepoint cellular proliferation was determined by MTS assay. Data are presented as mean ± SEM of n=3 patients and performed in triplicate. *** $p < 0.001$, significantly different by 2-way ANOVA. (**B**) Comparison of the effect of melatonin (120 pg/ml) on the proliferation of convex, concave and non-curve osteoblasts as determinbed by MTS assay. Data are presented as fold-change from 24h timepoint. *= $p < 0.05$, **= $p < 0.01$ *** $p < 0.001$, significant increase in cell number over the timecourse, as determined by 2-way ANOVA.

Figure 3. Convex osteoblasts from the curve apex exhibit increased oxidative metabolism. Primary convex, concave and non-curve osteoblasts from each of the

3 patients were subjected to a Mito Stress Test on the Seahorse XFe96 analyser. (**A**) Representative profile of the timecourse oygen Consumption Rate (OCR), where oliogomycin, FCCP, Antimycin A and rotenone are added sequentially. (**B**) Basal OCR (pmol/min) as a measure of basal respiration. Data are presented as mean ± SEM from 6 replicates per cell type in each of the 3 patients. (**C**) Maximal OCR (pmol/min) as a measure of maximal respiration. Data are presented as mean ± SEM from 6 replicates per cell type in each of the 3 patients. (**D**) Representative profile of extracellular acidification rate (ECAR), where where oliogomycin, FCCP, Antimycin A and rotenone are added sequentially. (**E**) Maximal ECAR (mpH/min/mg) as a measure of glycolytic capacity. Data are presented as mean ± SEM from 6 replicates per cell type in each of the 3 patients. * = $p < 0.05$, ** = $p < 0.01$, *** = $p < 0.001$, significantly different compared to non curve cells by 1-way ANOVA.

Figure 4. Convex osteoblasts from the curve apex exhibit greater bone mineralisation capacity. (**A**) Alkaline phosphatase activity of convex, concave and non-curve osteoblasts in culture over a timecourse of 8 days. Data represent mean ± SEM from n=3 patients. **= $p < 0.01$, ***=$p<0.001$, convex significantly from concave and non-curve osteoblasts at the same timepoint by 2-way ANOVA. (**B**) Relative quantification of bone nodule mineralisation of convex osteoblasts compared to concave osteoblasts upon culture in triplicate for 14 days after reaching confluence. Mineralisation was quantified by Alizarin Red staining. Bars represent mean relative mineralisation of n=3 patients ± SEM. *= $p< 0.05$.

Figure 5. Differential expression of wnt signalling mediators in osteoblasts at the curve apex

(**A**) mRNA expression of SKP2, SFRP1 and DKK1 in convex, concave and non-curve osteoblasts. Osteoblasts from n=3 patients were cultured in triplicate in 24-well plates and total RNA extracted using Trizol reagent. Relative expression was determined by ddCT method using Taqman probes and normalised to GAPDH. Data are presented as mean ± SEM from n=3 patients. *= $p < 0.05$, **= $p < 0.01$ by 1-way ANOVA. (**B**) Ingenuity Pathway Analysis of differentially expressed (>2-fold) wnt signalling genes illustrating the location of SFRP1 and SKP2 in the canonical wnt signalling pathway and their central role in wnt gene networks.

1 Negrini, S, De Mauroy, JC, Grivas, TB *et al.* Actual evidence in the medical approach to adolescents with idiopathic scoliosis. *Eur J Phys Rehabil Med 2014*;50:87-92.
2 Rainoldi, L, Zaina, F, Villafane, JH *et al.* Quality of life in normal and idiopathic scoliosis adolescents before diagnosis: reference values and discriminative validity of the SRS-22. A cross-sectional study of 1,205 pupils. *Spine J 2015*;15:662-7.
3 Zaina, F, De Mauroy, JC, Grivas, T *et al.* Bracing for scoliosis in 2014: state of the art. *Eur J Phys Rehabil Med 2014*;50:93-110.
4 Cheung, KM, Wang, T, Qiu, GX *et al.* Recent advances in the aetiology of adolescent idiopathic scoliosis. *Int Orthop 2008*;32:729-34.
5 Dickson, RA. The aetiology of spinal deformities. *Lancet 1988*;1:1151-5.
6 Newton Ede, MM & Jones, SW. Adolescent idiopathic scoliosis: evidence for intrinsic factors driving aetiology and progression. *Int Orthop 2016*;40:2075-80.
7 Cheng, JC, Qin, L, Cheung, CS *et al.* Generalized low areal and volumetric bone mineral density in adolescent idiopathic scoliosis. *J Bone Miner Res 2000*;15:1587-95.
8 Cheng, JC, Tang, SP, Guo, X *et al.* Osteopenia in adolescent idiopathic scoliosis: a histomorphometric study. *Spine (Phila Pa 1976) 2001*;26:E19-23.
9 Suh, KT, Lee, SS, Hwang, SH *et al.* Elevated soluble receptor activator of nuclear factor-kappaB ligand and reduced bone mineral density in patients with adolescent idiopathic scoliosis. *Eur Spine J 2007*;16:1563-9.
10 Cheng, JC, Hung, VW, Lee, WT *et al.* Persistent osteopenia in adolescent idiopathic scoliosis--longitudinal monitoring of bone mineral density until skeletal maturity. *Stud Health Technol Inform 2006*;123:47-51.
11 Cheung, CS, Lee, WT, Tse, YK *et al.* Generalized osteopenia in adolescent idiopathic scoliosis--association with abnormal pubertal growth, bone turnover, and calcium intake? *Spine (Phila Pa 1976) 2006*;31:330-8.
12 Lam, TP, Hung, VW, Yeung, HY *et al.* Abnormal bone quality in adolescent idiopathic scoliosis: a case-control study on 635 subjects and 269 normal controls with bone densitometry and quantitative ultrasound. *Spine (Phila Pa 1976) 2011*;36:1211-7.
13 Eun, IS, Park, WW, Suh, KT *et al.* Association between osteoprotegerin gene polymorphism and bone mineral density in patients with adolescent idiopathic scoliosis. *Eur Spine J 2009*;18:1936-40.
14 Man, GC, Wang, WW, Yeung, BH *et al.* Abnormal proliferation and differentiation of osteoblasts from girls with adolescent idiopathic scoliosis to melatonin. *J Pineal Res 2010*;49:69-77.
15 Machida, M, Dubousset, J, Imamura, Y *et al.* Pathogenesis of idiopathic scoliosis: SEPs in chicken with experimentally induced scoliosis and in patients with idiopathic scoliosis. *J Pediatr Orthop 1994*;14:329-35.
16 Machida, M, Dubousset, J, Imamura, Y *et al.* Melatonin. A possible role in pathogenesis of adolescent idiopathic scoliosis. *Spine (Phila Pa 1976) 1996*;21:1147-52.
17 Machida, M, Dubousset, J, Satoh, T *et al.* Pathologic mechanism of experimental scoliosis in pinealectomized chickens. *Spine (Phila Pa 1976) 2001*;26:E385-91.
18 Machida, M, Saito, M, Dubousset, J *et al.* Pathological mechanism of idiopathic scoliosis: experimental scoliosis in pinealectomized rats. *Eur Spine J 2005*;14:843-8.
19 Bradford, MM. A rapid and sensitive method for the quantitation of microgram quantities of protein utilizing the principle of protein-dye binding. *Anal Biochem 1976*;72:248-54.
20 Gregory, CA, Gunn, WG, Peister, A *et al.* An Alizarin red-based assay of mineralization by adherent cells in culture: comparison with cetylpyridinium chloride extraction. *Anal Biochem 2004*;329:77-84.
21 Philp, AM, Collier, RL, Grover, LM *et al.* Resistin promotes the abnormal Type I collagen phenotype of subchondral bone in obese patients with end stage hip osteoarthritis. *Sci Rep 2017*;7:4042.

22 Chang, J, Jackson, SG, Wardale, J *et al.* Hypoxia modulates the phenotype of osteoblasts isolated from knee osteoarthritis patients, leading to undermineralized bone nodule formation. *Arthritis Rheumatol 2014*;66:1789-99.
23 Brodner, W, Krepler, P, Nicolakis, M *et al.* Melatonin and adolescent idiopathic scoliosis. *J Bone Joint Surg Br 2000*;82:399-403.
24 Suh, KT, Lee, SS, Kim, SJ *et al.* Pineal gland metabolism in patients with adolescent idiopathic scoliosis. *J Bone Joint Surg Br 2007*;89:66-71.
25 Cheuk, KY, Zhu, TY, Yu, FW *et al.* Abnormal Bone Mechanical and Structural Properties in Adolescent Idiopathic Scoliosis: A Study with Finite Element Analysis and Structural Model Index. *Calcif Tissue Int 2015*;97:343-52.
26 Li, XF, Li, H, Liu, ZD *et al.* Low bone mineral status in adolescent idiopathic scoliosis. *Eur Spine J 2008*;17:1431-40.
27 Bovolenta, P, Esteve, P, Ruiz, JM *et al.* Beyond Wnt inhibition: new functions of secreted Frizzled-related proteins in development and disease. *J Cell Sci 2008*;121:737-46.
28 Uren, A, Reichsman, F, Anest, V *et al.* Secreted frizzled-related protein-1 binds directly to Wingless and is a biphasic modulator of Wnt signaling. *J Biol Chem 2000*;275:4374-82.
29 Bu, XM, Zhao, CH & Dai, XW. Aberrant expression of Wnt antagonist SFRP1 in pancreatic cancer. *Chin Med J (Engl) 2008*;121:952-5.
30 Chang, L, Lei, X, Qin, YU *et al.* Expression and prognostic value of SFRP1 and beta-catenin in patients with glioblastoma. *Oncol Lett 2016*;11:69-74.
31 Caldwell, GM, Jones, C, Gensberg, K *et al.* The Wnt antagonist sFRP1 in colorectal tumorigenesis. *Cancer Res 2004*;64:883-8.
32 Chen, YZ, Liu, D, Zhao, YX *et al.* Aberrant promoter methylation of the SFRP1 gene may contribute to colorectal carcinogenesis: a meta-analysis. *Tumour Biol 2014*;35:9201-10.
33 Dees, C, Schlottmann, I, Funke, R *et al.* The Wnt antagonists DKK1 and SFRP1 are downregulated by promoter hypermethylation in systemic sclerosis. *Ann Rheum Dis 2014*;73:1232-9.
34 Svensson, A, Norrby, M, Libelius, R *et al.* Secreted frizzled related protein 1 (Sfrp1) and Wnt signaling in innervated and denervated skeletal muscle. *J Mol Histol 2008*;39:329-37.
35 Thacker, G, Kumar, Y, Khan, MP *et al.* Skp2 inhibits osteogenesis by promoting ubiquitin-proteasome degradation of Runx2. *Biochim Biophys Acta 2016*;1863:510-9.
36 Fujita, T, Azuma, Y, Fukuyama, R *et al.* Runx2 induces osteoblast and chondrocyte differentiation and enhances their migration by coupling with PI3K-Akt signaling. *J Cell Biol 2004*;166:85-95.
37 Thomas, DM, Johnson, SA, Sims, NA *et al.* Terminal osteoblast differentiation, mediated by runx2 and p27KIP1, is disrupted in osteosarcoma. *J Cell Biol 2004*;167:925-34.
38 Takarada, T, Hinoi, E, Nakazato, R *et al.* An analysis of skeletal development in osteoblast-specific and chondrocyte-specific runt-related transcription factor-2 (Runx2) knockout mice. *J Bone Miner Res 2013*;28:2064-9.
39 Komori, T. Regulation of osteoblast differentiation by Runx2. *Adv Exp Med Biol 2010*;658:43-9.
40 Prince, M, Banerjee, C, Javed, A *et al.* Expression and regulation of Runx2/Cbfa1 and osteoblast phenotypic markers during the growth and differentiation of human osteoblasts. *J Cell Biochem 2001*;80:424-40.
41 Vimalraj, S, Arumugam, B, Miranda, PJ *et al.* Runx2: Structure, function, and phosphorylation in osteoblast differentiation. *Int J Biol Macromol 2015*;78:202-8.
42 Hayes, M, Gao, X, Yu, LX *et al.* ptk7 mutant zebrafish models of congenital and idiopathic scoliosis implicate dysregulated Wnt signalling in disease. *Nat Commun 2014*;5:4777.
43 Andersen, MR, Farooq, M, Koefoed, K *et al.* Mutation of the Planar Cell Polarity Gene VANGL1 in Adolescent Idiopathic Scoliosis. *Spine (Phila Pa 1976) 2017*;42:E702-E7.

Table 1. Patient characteristics and the gross structural parameters of spinal facet bone tissue.

Cobb angle was determined by analysis of pre-operative x-ray radiographs. Gross structural parameters of facet bone tissue at the curve apex (convex and conave) and from outside the curve (non Curve) was determined by MicroCT. a= Bone Mineral Density (BMD) units g/cm^2. b=Trabecular Thickness (TbTh) units µm. c=Trabecular Number (TbN) units mm^{-1}.

	Age (yrs)	Cobb Angle	Non Curve				Convex				Concave			
			Site	BMD[a]	TbTh[b]	TbN[c]	Site	BMD[a]	TbTh[b]	TbN[c]	Site	BMD[a]	TbTh[b]	TbN[c]
Patient 1	13	105° T6-L1	L2	0.03	375	0.10	T9	0.13	366	0.24	T9	0.10	275	0.27
Patient 2	15	50°	L1	0.09	471	0.15	T9	0.11	580	0.13	T9	0.05	463	0.12
Patient 3	16	66° T6-T11	T12	0.06	379	0.16	T8	0.11	551	0.14	T8	0.07	517	0.12

Table 2. Differential expression of Wnt signalling genes in osteoblasts at the curve apex.

Total RNA from convex, concave and non curve osteoblasts from patient 2 was analysed in duplicate for the mRNA expression of 84 wnt signalling genes by qRT-PCR using a RT2 profiler gene array (Qiagen, UK) Relative expression was determined by ddCT and normalised to 18S.

Concave vs Non-Curve		Convex vs Non-Curve		Concave vs Convex	
Gene	**Fold-Change**	**Gene**	**Fold-Change**	**Gene**	**Fold-Change**
AXIN1	3.2	BTRC	-2.1	AXIN2	2.4
AXIN2	4.6	DAB2	2.4	DAB2	-2.1
CSNK1A1	2.1	DKK1	-3.2	DKK1	8.1
CTNNB1	2.0	FRAT1	3.7	FRZB	2.0
DAAM1	3.5	FZD8	4.9	FZD1	2.3
DKK1	2.5	PITX2	-6.8	FZD3	2.2
DVL1	2.4	PPARD	2.5	PITX2	7.2
FOSL1	3.1	SFRP1	-26.0	PRICKLE1	2.2
FRAT1	4.5	SFRP4	-3.7	SFRP1	10.9
FZD1	2.0	VANGL2	-2.2	SFRP4	2.4
FZD8	2.8	WISP1	-2.0	VANGL2	5.3
NFATC1	2.1	WNT1	2.9	WISP1	2.5
NLK	2.7	WNT5B	-2.1	WNT2B	2.5
PPARD	2.6	LEF1	-5.7	WNT5B	3.1
PRICKLE1	2.1	MYC	2.0	CCND1	2.3
RUVBL1	2.2	SKP2	2.5	CXADR	2.4
SFRP1	-2.4			MTSS1	2.1
TCF7	2.4				
TCF7L1	2.5				
VANGL2	2.4				
WNT1	4.5				
WNT2B	2.3				
WNT7A	6.9				
CCND1	2.2				
CXADR	2.2				
CYP4V2	2.2				
LEF1	-5.8				
SKP2	2.1				

Figure 1

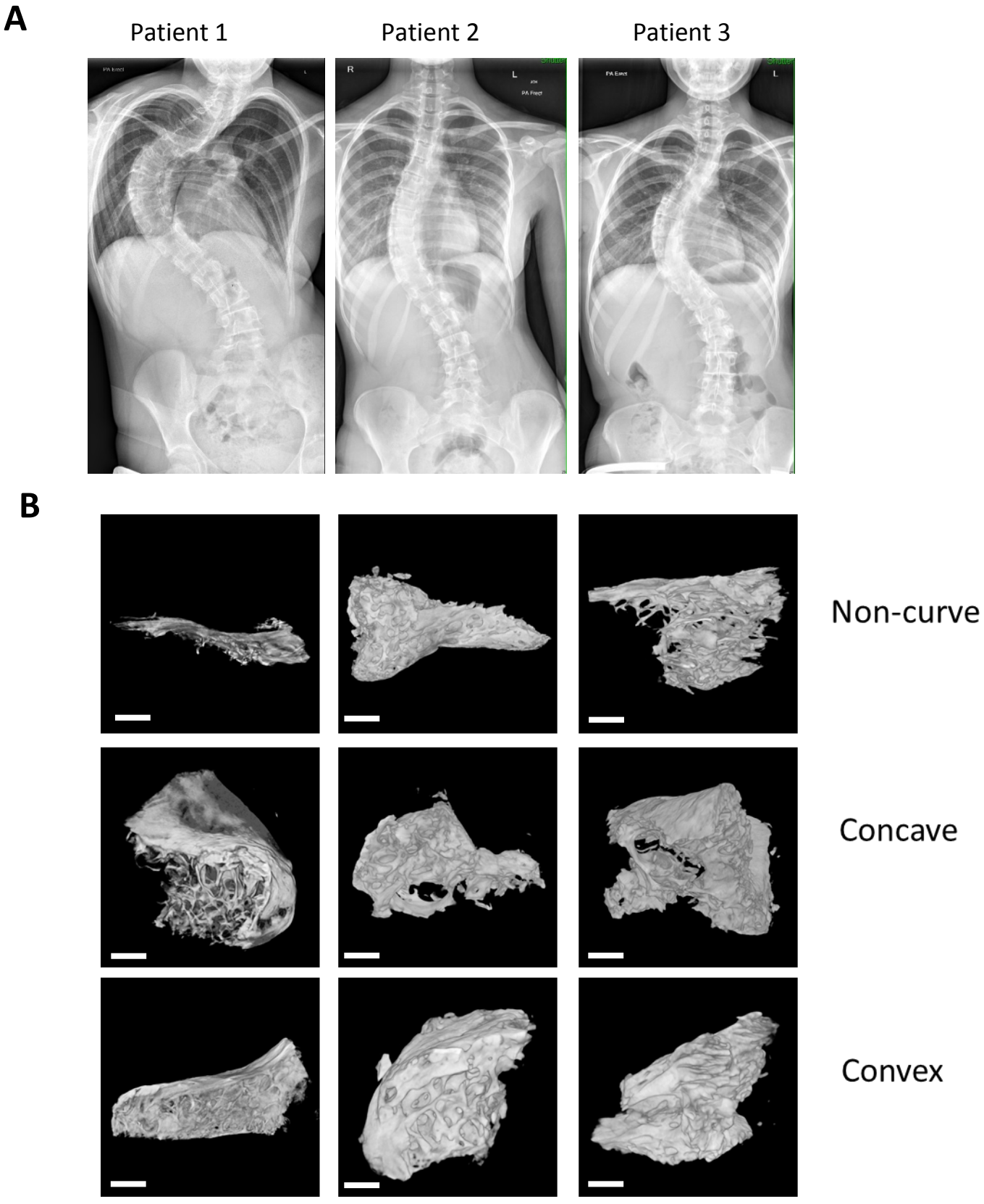

Figure 2

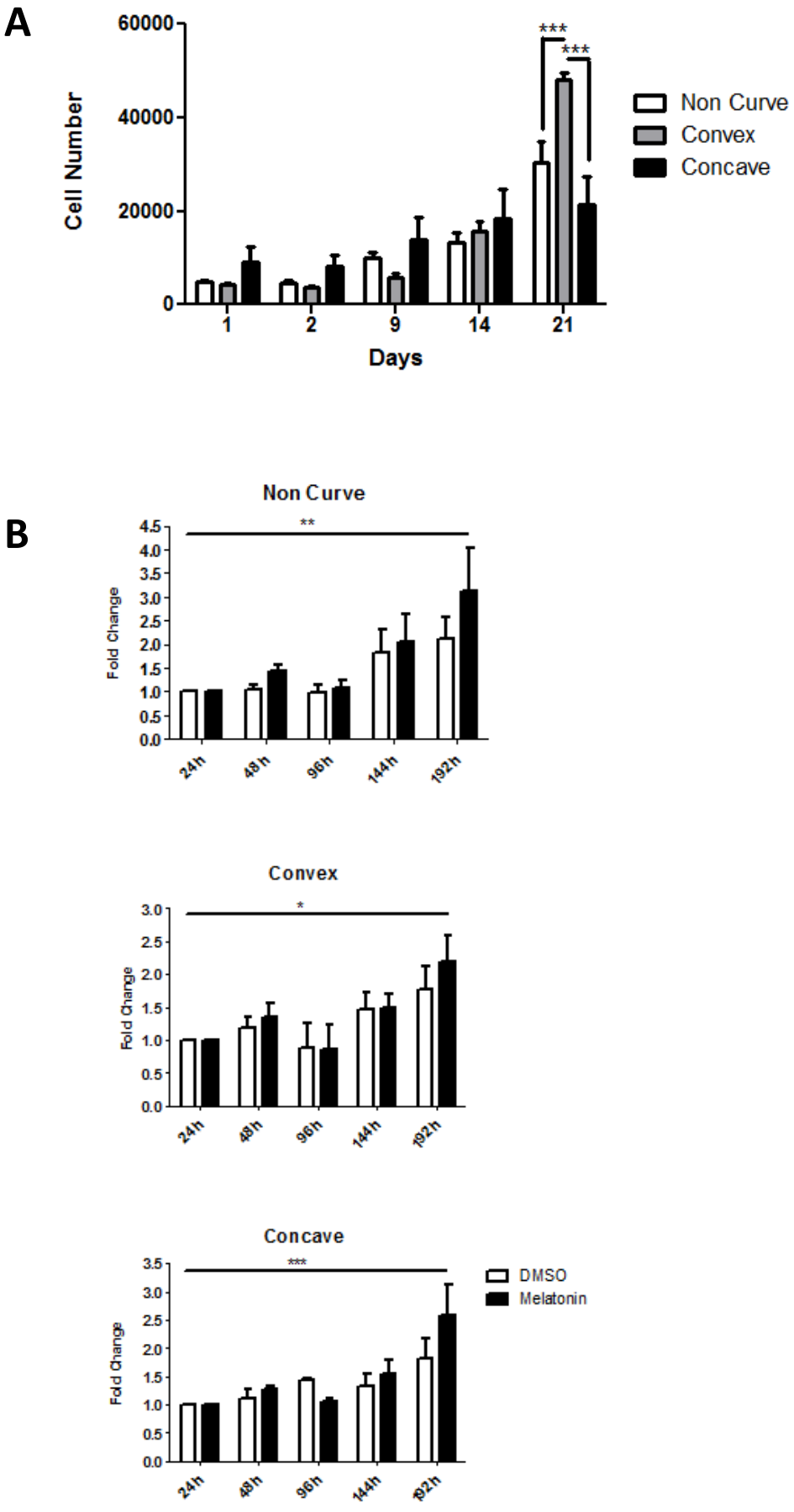
A
60000
40000
20000
0
Cell Number
1
2
9
14
21
Days
***
***
Non Curve
Convex
Concave
B
Non Curve
**
Fold Change
4.5
4.0
3.5
3.0
2.5
2.0
1.5
1.0
0.5
0.0
24h
48h
96h
144h
192h
Convex
*
Fold Change
3.0
2.5
2.0
1.5
1.0
0.5
0.0
24h
48h
96h
144h
192h
Concave
***
Fold Change
3.5
3.0
2.5
2.0
1.5
1.0
0.5
0.0
24h
48h
96h
144h
192h
DMSO
Melatonin

Figure 3

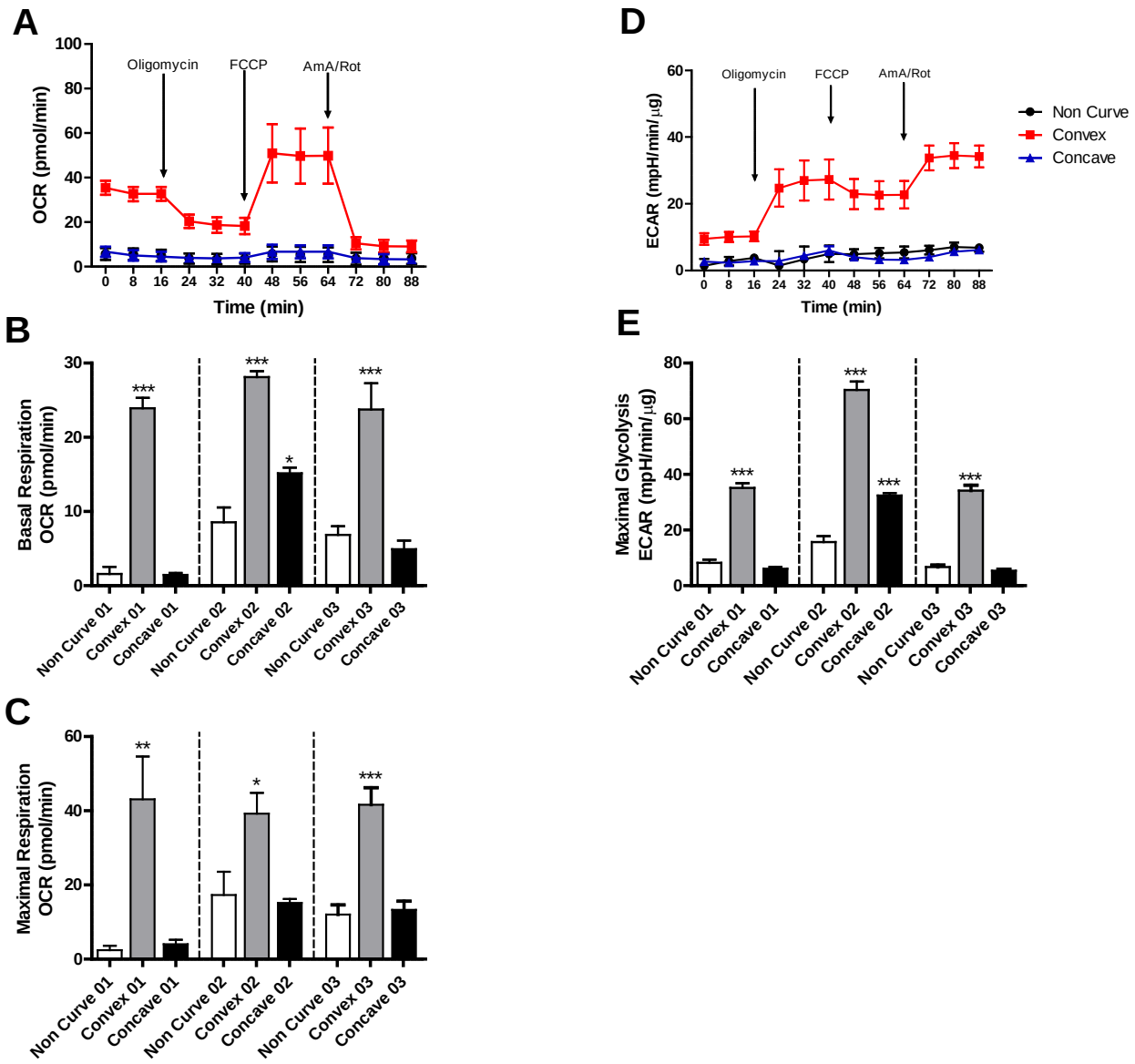
A
Oligomycin
FCCP
AmA/Rot
OCR (pmol/min)
Time (min)
D
ECAR (mpH/min/μg)
Non Curve
Convex
Concave
B
Basal Respiration OCR (pmol/min)
E
Maximal Glycolysis ECAR (mpH/min/μg)
C
Maximal Respiration OCR (pmol/min)
Non Curve 01
Convex 01
Concave 01
Non Curve 02
Convex 02
Concave 02
Non Curve 03
Convex 03
Concave 03

Figure 4

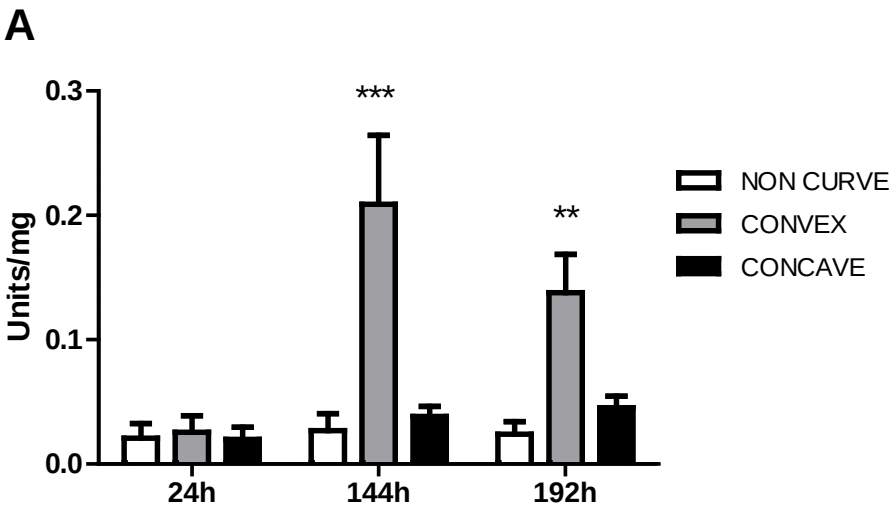
A
0.3
0.2
0.1
0.0
Units/mg
***
**
24h
144h
192h
NON CURVE
CONVEX
CONCAVE

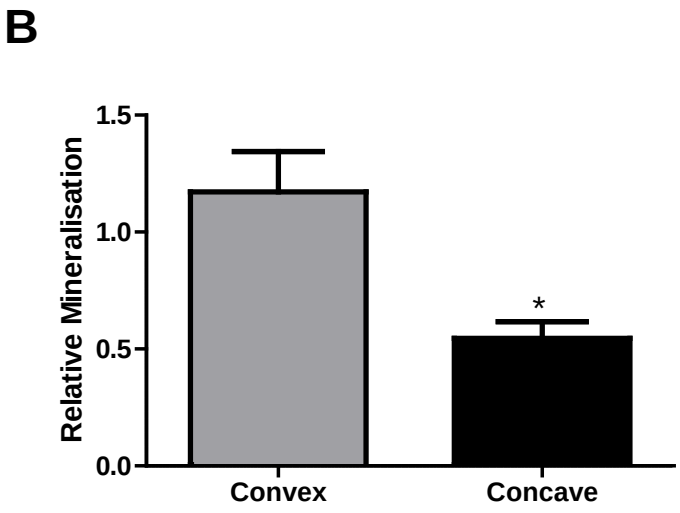
B
1.5
1.0
0.5
0.0
Relative Mineralisation
*
Convex
Concave

Figure 5

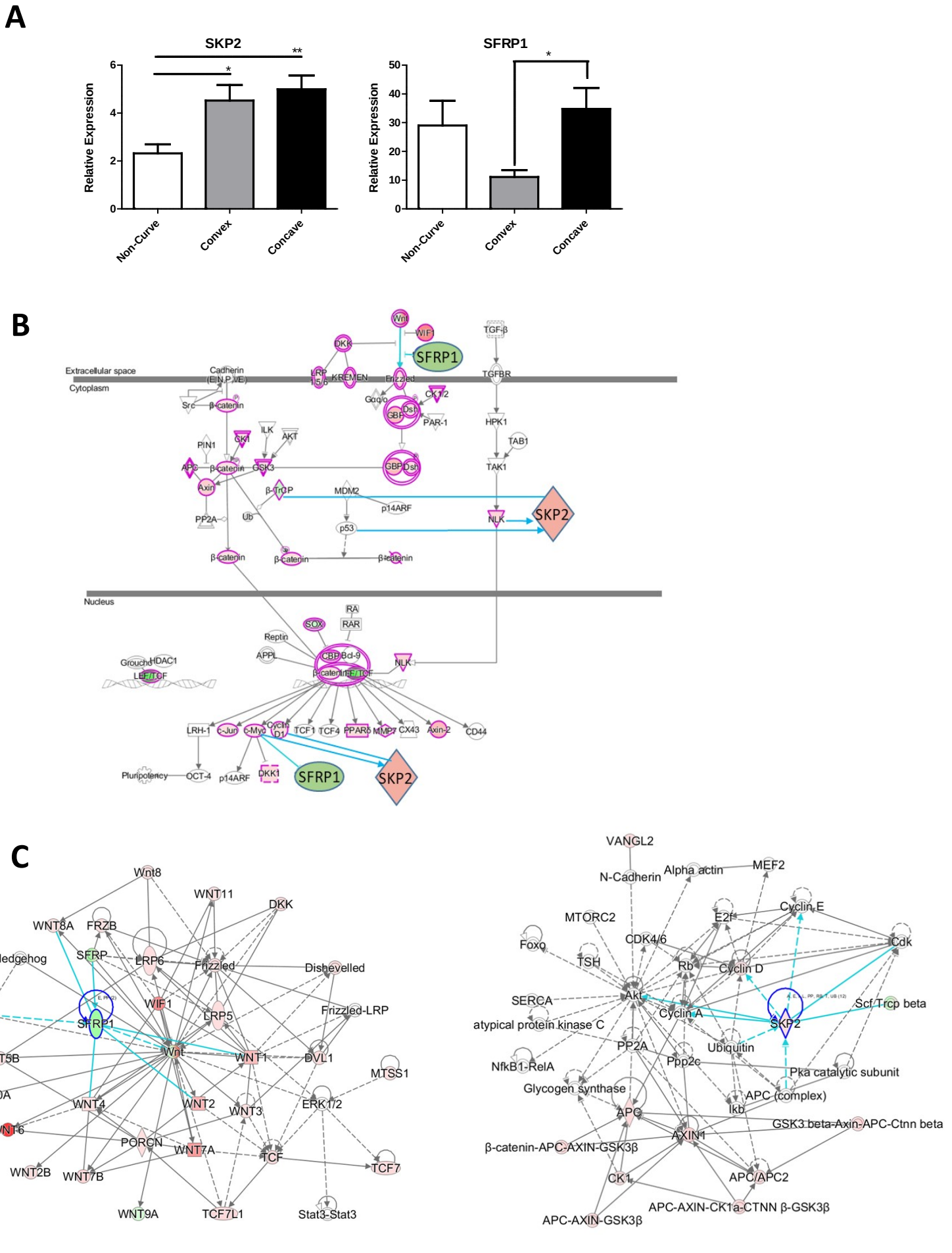
A
SKP2
SFRP1
Relative Expression
Non-Curve
Convex
Concave
B
Extracellular space
Cytoplasm
Nucleus
SFRP1
SKP2
C
Wnt8
WNT11
DKK
WNT8A
FRZB
Hedgehog
SFRP
LRP6
Frizzled
Dishevelled
WIF1
LRP5
Frizzled-LRP
Gli
WNT5B
Wnt
WNT1
DVL1
MTSS1
WNT10A
WNT4
WNT2
WNT3
ERK1/2
WNT6
PORCN
WNT7A
TCF
TCF7
WNT2B
WNT7B
WNT9A
TCF7L1
Stat3-Stat3
VANGL2
N-Cadherin
Alpha actin
MEF2
MTORC2
E2f
Cyclin E
Foxo
CDK4/6
Cdk
TSH
Rb
Cyclin D
SERCA
Akt
Cyclin A
Scf/Trcp beta
atypical protein kinase C
SKP2
PP2A
Ubiquitin
NfkB1-RelA
Ppp2c
Pka catalytic subunit
Glycogen synthase
APC (complex)
Ikb
APC
GSK3 beta-Axin-APC-Ctnn beta
AXIN1
β-catenin-APC-AXIN-GSK3β
CK1
APC/APC2
APC-AXIN-CK1a-CTNN β-GSK3β
APC-AXIN-GSK3β